

This is a repository copy of *Rapid compensatory evolution can rescue low fitness symbioses following partner-switching*.

White Rose Research Online URL for this paper:

<https://eprints.whiterose.ac.uk/id/eprint/175451/>

Version: Accepted Version

Article:

Sørensen, Megan E S, Wood, A. Jamie orcid.org/0000-0002-6119-852X, Cameron, Duncan D. et al. (1 more author) (2021) Rapid compensatory evolution can rescue low fitness symbioses following partner-switching. *Current Biology*. pp. 1-13. ISSN: 0960-9822

<https://doi.org/10.1016/j.cub.2021.06.034>

Reuse

This article is distributed under the terms of the Creative Commons Attribution-NonCommercial-NoDerivs (CC BY-NC-ND) licence. This licence only allows you to download this work and share it with others as long as you credit the authors, but you can't change the article in any way or use it commercially. More information and the full terms of the licence here: <https://creativecommons.org/licenses/>

Takedown

If you consider content in White Rose Research Online to be in breach of UK law, please notify us by emailing eprints@whiterose.ac.uk including the URL of the record and the reason for the withdrawal request.

Rapid compensatory evolution can rescue low fitness symbioses following partner-switching

Megan E S Sørensen¹, A Jamie Wood², Duncan D Cameron¹, Michael A Brockhurst^{3*}

1. Department of Animal and Plant Sciences, University of Sheffield, Sheffield S10 2TN
2. Department of Biology, University of York, York YO10 5DD
3. Division of Evolution and Genomic Sciences, School of Biological Sciences, University of Manchester, Manchester M13 9PT

*Lead contact Michael A. Brockhurst.

Email: michael.brockhurst@manchester.ac.uk

Twitter: @BrockhurstLab

Summary

Partner-switching plays an important role in the evolution of symbiosis, enabling local adaptation and recovery from the breakdown of symbiosis. Because of intergenomic epistasis, partner-switched symbioses may possess novel combinations of phenotypes but may also exhibit low fitness due to their lack of recent coevolutionary history. Here, we examine the structure and mechanisms of intergenomic epistasis in the *Paramecium-Chlorella* symbiosis and test if compensatory evolution can rescue initially low fitness partner-switched symbioses. Using partner-switch experiments coupled with metabolomics we show evidence for intergenomic epistasis wherein low fitness is associated with elevated symbiont stress responses either in dark or high irradiance environments, potentially owing to mismatched light management traits between the host and symbiont genotypes. Experimental evolution under high light conditions revealed that an initially low fitness partner-switched non-native host-symbiont pairing rapidly adapted, gaining fitness equivalent to the native host symbiont pairing in less than 50 host generations. Compensatory evolution took two alternative routes: Either, hosts evolved higher symbiont loads to mitigate for their new algal symbiont's poor performance, or the algal symbionts themselves evolved higher investment in photosynthesis and photoprotective traits to better mitigate light stress. These findings suggest that partner-switching combined with rapid compensatory evolution can enable the recovery and local adaptation of symbioses in response to changing environments.

Keywords: Symbiosis, Experimental evolution, photosymbiosis, partner-switching

Introduction

Beneficial symbioses have an inherent potential for conflict between the symbiotic partners. This can drive the breakdown of symbiosis if environmental conditions change the net benefit of interacting or if the pursuit of individual fitness favours cheating¹. Both situations can select for partner-switching to recombine symbiotic partnerships². Partner-switching can

provide hosts with access to favourable symbiotic phenotypes to overcome maladaptation to the prevailing environmental context³ or restore symbiont function following breakdown^{4,5}. The generation of phenotypic plasticity through partner-switching arises from genetic variation of hosts (G^H) and symbionts (G^S) and intergenomic epistasis⁶, that is, genetic variation for the outcome of symbiosis in the form of host genotype by symbiont genotype interactions ($G^H \times G^S$) for symbiotic traits or fitness. Furthermore, the fitness effects of symbiosis can be mediated by the environmental context⁷, causing host-genotype-by-symbiont-genotype-by-environment interactions ($G^H \times G^S \times E$). A consequence of $G^H \times G^S \times E$ interactions is that there is unlikely to be an optimal host-symbiont pairing across all environments, further driving selection for partner-switching or dynamic coevolution of the symbiosis⁸. As such, partner-switching can enable niche-expansion by hosts^{9,10} and provide a mechanism by which hosts can adapt to local environmental conditions faster than through *de novo* adaptation of the current symbiont^{11,12}.

Newly interacting partner-switched host-symbiont pairings are, however, unlikely to be co-adapted due to their lack of recent coevolutionary history and may, therefore, initially have low fitness^{13–15}. Indeed, despite the adaptive potential of partner-switching, new host-symbiont pairings, like genetic mutations, may more often be deleterious than beneficial to host fitness due to phenotypic mismatches or genetic incompatibilities. This has been observed in a range of symbiotic interactions: for example, a newly acquired *Symbiodinium* endosymbiont was found to translocate less fixed carbon than the native symbiont to its cnidarian host¹³; novel bacterial endosymbionts had reduced vertical transmission rates in aphid hosts¹⁴; and novel *Wolbachia* endosymbionts reduced the reproductive fitness of *Drosophila simulans*¹⁵. How then do newly-formed, poorly co-adapted host-symbiont pairings become stable, beneficial symbioses? We hypothesise that rapid compensatory evolution (that is adaptation of the host, the symbiont, or both to ameliorate the deleterious fitness effects of partner-switching) could allow partner-switched symbioses to overcome their initially low fitness. Indeed, there is some, albeit limited, experimental evidence to

support this idea: For example, the high fitness cost of newly acquired *Spiroplasma* endosymbionts in *Drosophila melanogaster* was ameliorated within only 17 host generations¹⁶, although the underlying mechanisms of this fitness recovery remain unknown. Furthermore, horizontal gene transfers were found to have caused the rapid evolution of nonsymbiotic strains of rhizobia bacterial symbionts into symbiotic partners in field-site tests with *Lotus* plant hosts¹⁷.

The microbial symbiosis between *Paramecium bursaria* and *Chlorella* provides an experimentally tractable model system to study intergenomic epistasis and the underlying molecular mechanisms. The ciliate host, *P. bursaria*, is a single-celled eukaryote, and each host cell contains 100-600 cells of the algal endosymbiont, *Chlorella*^{18,19}. The *P. bursaria* - *Chlorella* symbiosis is based on a primary nutrient exchange of fixed carbon from the photosynthetic alga for organic nitrogen from the heterotrophic host^{18,20}. *Chlorella* algal symbionts are primarily vertically transmitted to daughter cells at *Paramecium* cell division, although additional algal symbionts can also be acquired from the environment by ingestion^{21,22}. This symbiosis is geographically widespread and genetically diverse, in part due to multiple independent acquisitions of algal symbionts by *P. bursaria*. The primary nutrient exchange is convergent among these origins²³. This facilitates partner-switching, but concurrent divergence in other metabolic traits can cause phenotypic mismatches in partner-switched host-symbiont pairings²³. Here, using experimental partner-switches, we examined the pattern and mechanisms of intergenomic epistasis for three diverse host-symbiont strains, observing significant $G^H \times G^S \times E$ interactions for host-symbiont growth rate and symbiont load (that is the number of symbionts per host cell), together with corresponding differences in metabolism. We then experimentally evolved a low fitness partner-switched host-symbiont pairing for ~50 host generations. We observed rapid compensatory evolution by hosts and symbionts that improved fitness to equal to that of the native host-symbiont pairing mediated by evolved changes in host control of symbiont load and in symbiont metabolism.

Results

Intergenomic epistasis for host-symbiont growth and symbiont load. We constructed all possible host-symbiont genotype pairings ($n = 9$) of 3 diverse strains of *Paramecium-Chlorella* and confirmed their identity by diagnostic PCR (Figure S1). We measured the growth reaction norm of each host-symbiont pairing across a light gradient (Figure 1a). All host-symbiont pairings showed the classic photosymbiotic reaction norm²⁴, such that growth rate increased with irradiance, but we observed a significant $G^H \times G^S \times E$ interaction for host-symbiont growth rate ($G^H \times G^S \times E$ interaction, ANOVA, $F_{17,162} = 18.81$, $P < 0.001$) consistent with intergenomic epistasis. This was driven by contrasting effects of symbiont genotype on growth in the different host backgrounds across light environments. In the HK1 and HA1 host-backgrounds, similar growth reaction norms with light were observed for each symbiont genotype, whereas in the 186b host background the growth reaction norm varied according to symbiont genotype. Interestingly, the native 186b host-symbiont pairing had both the lowest intercept and the highest slope, indicating that in the 186b host background the native algal symbiont genotype was costlier in the dark (Welch t-test on native versus non-native symbionts $t(7.29) = -10.13$, $p = < 0.001$) yet more beneficial in high-light environments than non-native algal symbiont-genotypes (Welch t-test on native versus non-native symbionts $t(10.44) = 3.21$, $p = < 0.01$).

P. bursaria host cells regulate their algal symbiont load (i.e. the number of symbionts per host cell) according to light irradiance to maximise the benefit-to-cost ratio of symbiosis, such that, for naturally occurring host-symbiont pairings, symbiont load peaks at intermediate irradiance and is reduced both in the dark and at high irradiance^{24–26}. To test if regulation of symbiont load varied among host-symbiont pairings, we measured symbiont load across the light gradient as the intensity of single-cell fluorescence, which is correlated with the number of symbionts per host cell¹⁹, by flow cytometry (Figure 1b). All host-symbiont pairings showed the expected unimodal symbiont load curve with light, but

nevertheless we observed a significant $G^H \times G^S \times E$ interaction for symbiont load ($G^H \times G^S \times E$ interaction, ANOVA, $F_{17,162} = 3.78$, $P < 0.001$) consistent with intergenomic epistasis. Whereas, in the HA1 host similar symbiont load reaction norms were observed for each symbiont genotype, for the HK1 and 186b host backgrounds the form of the symbiont load reaction norms varied according to symbiont genotype. In the HK1 host, the magnitude of the symbiont load varied by symbiont genotype, such that higher symbiont loads were observed for the native compared to the non-native symbiont-genotypes. In the 186b host, peak symbiont load occurred at different light levels according to symbiont genotype, such that for the native symbiont the symbiont load curve peaked at a higher light intensity when compared to the non-native symbionts. (For the full output of the polynomial model, see Data S1.) Because symbiont load is primarily host-controlled in this system^{24,25}, this suggests that the HK1 and 186b host-genotypes discriminated among symbiont-genotypes, and then regulated symbiont load accordingly.

Metabolic mechanisms of intergenomic epistasis. To investigate the potential metabolic mechanisms underlying the observed intergenomic epistasis we performed untargeted global metabolomics with ESI-ToF-MS independently for the host and symbiont metabolite fractions for each host-symbiont pairing across the light gradient²³. Light irradiance was the primary driver of differential metabolism for both host and symbiont, however, host-dependent differences in the metabolism of symbiont-genotypes could be detected. For the symbiont metabolite fraction subset by host-genotype, we observed native versus non-native clustering of symbiont metabolism only when associated with the 186b host-genotype (Figure S2). This is consistent with the larger phenotypic differences in growth and symbiont load observed among host-symbiont pairings with the 186b host-genotype compared to with either the HK1 or HA1 host-genotypes. We therefore focused our analyses on comparing the metabolic profiles of the different symbiont genotypes within the 186b host background. Pairwise contrasts of the symbiont-genotypes in the 186b host-genotype background revealed a range of candidate symbiont metabolites which distinguished the native pairing

from either non-native host-symbiont pairing. Putative identifications included, in the dark, elevated levels of candidate metabolites associated with stress responses (stress-associated hormones, jasmonic acid and abscisic acid, and stress associated-fatty acids, such as arachidonic acid) but reduced production of vitamins and co-factors by the native symbiont, compared to the non-native symbionts (Table S1). At high irradiance, the native symbiont showed higher levels of candidate metabolites in central metabolism, hydrocarbon metabolism and of biotin (vitamin B7), compared to the non-native symbionts (Table S1). In contrast, the non-native symbionts produced elevated levels, relative to native symbionts, of a candidate glutathione derivative; glutathione is an antioxidant involved in the ascorbate-glutathione cycle that combats high UV stress through radical oxygen scavenging^{27,28}. Together, these data suggest that impaired host-symbiont performance was associated with elevated symbiont stress responses and that symbiont genotypes varied in their requirement for host photoprotection, providing a putative mechanism underlying intergenomic epistasis.

Rapid compensatory evolution can rescue an initially low fitness partner-switched symbiosis. The partner-switched pairing of the 186b host with the HK1 symbiont showed substantially reduced growth at high light relative to the native 186b host-symbiont pairing. To test if this fitness deficit could be overcome through compensatory evolution, we established six replicate populations of each of these two symbiotic partnerships (i.e., the 186b host with the 186b algal symbiont and the 186b host with the HK1 algal symbiont), which were propagated by weekly serial transfer for 25 transfers (approximately 50 host generations) at a high light regime (50 μ E; 14:10 L:D). The growth rate per transfer was higher for the native pairing than the non-native pairing (Figure S3a) (linear mixed effect model, HK1 symbiont fixed effect of -0.08 ± 0.006 , T-value = -14.126 , see Data S1 for full statistical output), but increased over time for both pairings (transfer number fixed effect 0.001 ± 0.0004 , T-value = 3.088). To test for adaptation, we compared the fitness effect of symbiosis at the beginning and the end of the transfer experiment by direct competition of either the ancestral or evolved host-symbiont pairings against the symbiont-free ancestral

186b host genotype across a light gradient. Fitness at the start of the evolution experiment of symbiotic relative to non-symbiotic hosts increased more steeply with irradiance for the native than the partner-switched non-native pairing (Figure 2), but this difference had disappeared by the end of the evolution experiment, such that both the native and non-native host-symbiont pairings showed increasing fitness relative to non-symbiotic hosts with increasing irradiance (symbiont genotype by light intensity by transfer number interaction term: ANOVA, $F_{7,45}=6.20$, $P<0.001$). Indeed, at $50 \mu\text{E m}^{-2} \text{s}^{-1}$, the light level used in the selection experiment, the large fitness deficit observed between the native and non-native pairing at the beginning of the experiment had been completely compensated. Comparison of the growth reaction norms of the evolving populations over time suggested that this amelioration occurred rapidly: By the tenth transfer, the native and non-native host-symbiont pairings showed equivalent growth responses to light (Welch t-test $t(45.96) = -0.26$, $p = 0.80$), in contrast to their substantially different ancestral growth reaction norms observed at the start of the evolution experiment (Welch t-test $t(35.79) = 3.59$, $p = <0.001$) (Figure S3b). These data suggest that newly established partner-switched symbioses can rapidly achieve equivalent growth performance and fitness benefits as the native host-symbiont pairing by compensatory evolution.

Evolved changes in symbiont load regulation and metabolism. To understand the mechanisms of compensatory evolution, we first compared the symbiont load reaction norms of the ancestral and evolved native and non-native pairings (Figure 3). Both ancestral host-symbiont pairings showed the expected unimodal symbiont load curve with light, albeit with higher symbiont loads for the native compared to the non-native pairing at the highest light level, $50 \mu\text{E m}^{-2} \text{s}^{-1}$ irradiance, as used in the transfer experiment. By the end of the evolution experiment, the shape of the symbiont load reaction norms were altered in both the native and non-native pairings. Most notably, at $50 \mu\text{E m}^{-2} \text{s}^{-1}$ irradiance, whereas the non-native pairing had increased symbiont load, symbiont load had decreased in the native pairing, such that symbiont load was now higher in the non-native pairing (transfer by

symbiont genotype interaction at high light: ANOVA, $F_{3,20} = 16.88$, $P < 0.001$). Higher symbiont loads may therefore have contributed to the observed increased fitness of evolved compared to ancestral non-native pairings in the high light environment.

Next, to investigate the potential underlying metabolic mechanisms, we performed untargeted metabolomics analyses on the separated *Chlorella* and *P. bursaria* fractions from samples taken the start and end of the evolution experiment grown at $50 \mu\text{E m}^{-2} \text{s}^{-1}$. The ancestral *P. bursaria* and *Chlorella* metabolic profiles of native and non-native host-symbiont pairings could be clearly distinguished (Figure 4). At the end of the evolution experiment, *P. bursaria* metabolism displayed a high degree of apparent convergence between hosts evolved with the native versus the non-native symbionts (Figure 4a,c). This was driven by decreased levels of compounds of central metabolism (such as pyruvate and TCA cycle intermediates, antioxidants, lipids, and some amino acids) (Table S2), suggesting either increased pathway completion or a reduced metabolic rate, both of which can lead to increased efficiency. In addition, we observed increased levels of the amino acid cysteine and a shikimate pathway component in hosts evolved with the native versus the non-native symbionts (Figure S4). Levels of algal-cell degradation components (Figure S4), such as cell-wall degradation product chitotriose, were increased in some replicates of hosts evolved with either symbiont, potentially suggesting increased digestion of *Chlorella*, which is a known mechanism by which hosts control their symbiont load^{29,30}.

In contrast, evolved changes to the metabolic profiles of the algal symbiont genotypes showed less consistent differences among treatments (Figure 4b,d). Whereas all replicates of the native 186b *Chlorella* evolved in a similar direction, the replicates of the non-native HK1 *Chlorella* evolved in two different directions. Two of the HK1 replicates took a similar trajectory to the 186b symbionts, while the remaining four replicates all followed an alternative evolutionary trajectory. The group of four HK1 replicates that diverged during the experiment had lower production of metabolites within core aspects of metabolism, such as

lipids, amino acids and carbohydrates. The second group, including the remaining two HK1 replicates and all the 186b replicates, had for the most part higher production of metabolites within primary metabolism pathways, particularly within lipids and carbohydrates, as well as a key chlorophyll compound, a photo-protective carotenoid (though not for all of the 186b replicates), and secondary metabolites with potential antioxidant properties (Figure S4, Table S2). This greater investment into photosynthesis and photo-protection may improve carbon transfer to the host^{31,32}, and decrease light stress, which aligns with the decrease in host antioxidants. Interestingly, the two HK1 replicates that appeared to converge metabolically with the native symbionts had a lower increase in symbiont load compared to the replicates that metabolically diverged (Table S3). This implies that the evolution of metabolism and symbiont load were linked, and that overall two alternative strategies of compensatory evolution emerged: either to have fewer, more beneficial symbionts or to have more, less-beneficial symbionts.

Discussion

Partner switching plays an important role in the evolution of a wide range of symbioses^{2,4,5,33,34} enabling adaptation to changing environments and recovery from the breakdown of symbiosis. Because of intergenomic epistasis, partner-switched host-symbiont pairings may possess novel adaptive phenotypes, but will sometimes exhibit low fitness associated with mismatches between host and symbiont traits, owing to their lack of recent coevolutionary history^{14,15,35}. In the *Paramecium-Chlorella* symbiosis, low fitness host symbiont pairings were associated with elevated symbiont stress responses either in dark or high irradiance environments, suggesting that mismatching light management traits between host and symbiont genotypes may be a potential cause of intergenomic epistasis. This corresponds with findings from other photosynthetic symbioses, including coral-*Symbiodinium* and *Hydra-Chlorella*, where mismatching thermal and light stress tolerances contribute to the breakdown of symbiosis^{36–39}. Low fitness, partner-switched host-symbiont pairings were rescued by compensatory evolution, which took one of two routes: Either, hosts evolved

higher symbiont loads to mitigate for their new algal symbiont's poor performance, or the algal symbionts themselves evolved higher investment in photosynthesis and photoprotection traits to better mitigate light stress. Given that symbiont load varies with light due to host control^{24,25}, it seems likely that the evolved change in symbiont load is due to phenotypic plasticity through altered host regulation, whereas the evolved change in algal photosynthetic metabolism could be due to either genetic or physiological adaptation by the symbionts. Both strategies increased growth of the non-native host-symbiont pairing, leading to higher fitness equivalent to that of the native host-symbiont pairing. Together, these data suggest that, partner-switching combined with rapid compensatory evolution can contribute to the recovery of symbiosis and local adaptation of hosts to changing environmental conditions. Partner-switching combined with rapid compensatory evolution could thus enhance the resilience of symbioses to environmental change, enabling the maintenance of their contribution to ecosystem function. Moreover, the potential fitness benefits of the phenotypic plasticity provided by partner-switching may select against the evolution of strict vertical transmission in symbioses that inhabit fluctuating or rapidly changing environments.

Acknowledgements

This work was funded by grants NE/K011774/2 and NE/V000128/1 from the Natural Environment Research Council, UK to M.A.B, D.D.C, and A.J.W and a White Rose DTP studentship from the Biotechnology and Biological Sciences Research Council, UK (BB/011151/1) to M.E.S.S. The funders had no role in the design of the study, the collection, analysis and interpretation of data or writing of the manuscript. We are grateful to Heather Walker for her technical assistance with the mass spectrometry.

Author Contributions: M.A.B, D.D.C, and M.E.S.S conceived and designed the study. M.E.S.S conducted experimental work. M.E.S.S and D.D.C analysed the data. M.E.S.S and M.A.B drafted the manuscript. All authors commented on the manuscript.

Declaration of Interests: The authors declare no competing interests.

Figure Legends

Figure 1. Intergenomic epistasis of host symbiont growth rate and symbiont load reaction norms. For both A and B, each panel presents the data for a specific genotype of *P. bursaria* host, as indicated at top of each panel, and the symbiont genotypes are distinguished by colour. A) Initial growth rates of the host-symbiont pairings across a light gradient over three days. The data points show the mean (n=3) initial growth rate \pm SE. The host-symbiont growth rate reaction norm varied by symbiont genotype in the 186b host genotype but did not vary in the HA1 or HK1 host genotypes, consistent with intergenomic epistasis. B) Symbiont load of the host-symbiont pairings across a light gradient. The data points show the mean (n=3) symbiont load, measured as relative chlorophyll fluorescence, \pm SE. The lines show polynomial models; the model coefficients showed a significant $G^H \times G^S$ interaction (ANOVA, $F_{8,36} = 27.22$ (the intercept); 8.58 (first coefficient); 6.09 (second coefficient), $P < 0.001$). For full statistical output see Data S1. The symbiont load reaction norm varied by symbiont genotype in both the HK1 and 186b host genotypes but did not vary in the HA1 host genotype, consistent with intergenomic epistasis. Related to Figure S2 and Table S1.

Figure 2. Relative fitness reaction norms at the start and end of the evolution experiment. Panels show relative fitness reaction norms across a light gradient of various host-symbiont pairings in the 186b host genotype in direct competition with the symbiont-free 186b host genotype. The left-hand panel shows fitness reaction norms measured at the start of the evolution experiment (T0) and the right-hand panel shows fitness reaction norms measured at the end of the evolution experiment (T25), as indicated at the top of each panel. Relative fitness was calculated as the selection rate, where a value above 0 indicates a fitness benefit to the host of carrying algal symbionts. Colours show the symbiont genotype treatment, where blue denotes that the 186b host carried the native 186b symbiont genotype whereas grey denotes that the 186b host carried the non-native HK1 symbiont genotype. Dark, thick lines show the mean (n=6) relative fitness reaction norms and light, thin lines show the relative fitness reaction norms for each individual replicate. At the start of the evolution experiment only the native host-symbiont pairing showed an increasing fitness benefit of carrying symbionts with increasing irradiance, whereas at the end of the evolution experiment both the native and non-native host symbiont pairings showed an increasing fitness benefit of carrying symbionts with increasing irradiance. Related to Figure S3.

Figure 3. Symbiont load reaction norms at the start and end of the evolution

experiment. Panels show symbiont load reaction norm across a light gradient of various host-symbiont pairings in the 186b host genotype. The left-hand panel shows symbiont load reaction norms measured at the start of the evolution experiment (T0) and the right-hand panel shows symbiont load reaction norms measured at the end of the evolution experiment (T25), as indicated at the top of each panel. Colours show the symbiont genotype treatment, where blue denotes that the 186b host carried the native 186b symbiont genotype whereas grey denotes that the 186b host carried the non-native HK1 symbiont genotype. Symbols show the mean ($n=6$) \pm standard error symbiont load and lines show the symbiont load reaction norms for each individual replicate. At the irradiance level used in the evolution experiment ($50 \mu\text{E m}^{-2} \text{ s}^{-1}$), we observed that whereas mean symbiont load of the native symbiont had reduced, symbiont load of the non-native symbiont had increased, by the end of the evolution experiment. Related to Figure S3 and Table S3.

Figure 4. Evolutionary trajectories of *Paramecium* and *Chlorella* metabolism. Panels A and C show PCA plots for *P. bursaria* metabolism, while panels B and D show PCA plots for *Chlorella* metabolism, as indicated in the panel labels. The top row (A and B) plot PC1 versus PC2. The bottom row (C and D) plot PC2 versus PC3. The percent variation explained by each PC is shown on the associated axis label. Colours show the symbiont genotype treatment, where blue denotes that the 186b host carried the native 186b symbiont genotype whereas grey denotes that the 186b host carried the non-native HK1 symbiont genotype. Dark points show ancestral metabolism at the state of the evolution experiment (mean of $n=6$) whereas light points show the metabolism of each individual replicate population at the end of the evolution experiment (mean of $n=3$ technical replicates per population). Arrows show the trajectory of metabolic evolution followed by each replicate population during the evolution experiment, and 95% confidence ellipses have been drawn for each treatment. The metabolite identifications for the top loadings are shown in their corresponding location. Related to Figure S4 and Table S2 & S3.

350 **STAR Methods**

351 **Resource availability**

352 **Lead contact**

353 Further information and requests for resources and reagents should be directed to and will
354 be fulfilled by the Lead Contact, Michael Brockhurst
355 (michael.brockhurst@manchester.ac.uk).

356

357 **Materials availability**

358 The natural strains used in this paper are available from culture collections (see below),
359 unfortunately all our experimental populations were lost during the lab closures at the
360 beginning of the global Covid pandemic.

361

362 **Data and code availability**

363 The data has been deposited within Mendeley Data (DOI: 10.17632/m7tpztyjx.1).

364

365 **Experimental Model and Subject Details**

366 The three natural strains of symbiotic *P. bursaria* used were: 186b (CCAP 1660/18) obtained
367 from the Culture Collection for Algae and Protozoa (Oban, Scotland), and HA1 and HK1
368 isolated in Japan and obtained from the Paramecium National Bio-Resource Project
369 (Yamaguchi, Japan). *P. bursaria* stock cultures were maintained at 25°C under a 14:10 L:D
370 cycle with 50 $\mu\text{E m}^{-2} \text{s}^{-1}$ of light (a high light condition). The stocks were maintained by batch
371 culture in bacterized Protozoan Pellet Media (PPM, Carolina Biological Supply), made to a
372 concentration of 0.66 g L⁻¹ with Volvic natural mineral water, and inoculated approximately
373 20 hours prior to use with *Serratia marcescens* from frozen glycerol stocks.

374

375 To isolate *Chlorella* from the symbiosis, symbiotic cultures were first washed and
376 concentrated with a 11 μm nylon mesh using sterile Volvic. The suspension was then
377 ultrasonicated using a Fisherbrand™ Q500 Sonicator (Fisher Scientific, NH, USA), at a
378 power setting of 20% for 10 seconds sonification to disrupt the host cells. The liquid was
379 then spotted onto Bold Basal Media plates (BBM)⁴⁰, from which green colonies were

streaked out and isolated over several weeks. Plate stocks were maintained by streaking out one colony to a fresh plate every 3/4 weeks.

Symbiont-free *P. bursaria* were made by treating symbiotic cultures with paraquat (10 µg mL⁻¹) for 3 to 7 days in high light conditions (>50 µE m⁻² s⁻¹), until the host cells were visibly symbiont free. The cultures were then extensively washed with Volvic and closely monitored with microscopy and flow cytometry over a period of several weeks to check that re-greening by *Chlorella* did not occur. Stock cultures of the symbiont-free cells were maintained by batch culture at 25°C under a 14:10 L:D cycle with 3 µE m⁻² s⁻¹ of light and were given fresh PPM weekly. Symbiont-free *Paramecium* stocks have been maintained for a substantial period of time (months/years) without *Chlorella* ever being observed either inside or outside of *Paramecium* cells. In addition, using flow cytometry we have never observed chlorophyll fluorescence for *Paramecium* cells sampled from these stocks (methodology detailed in symbiont Load section). Together these tests confirm that paraquat treatment successfully removes all of the native *Chlorella*.

Method Details

Cross infection

Symbiont-free populations of the three *P. bursaria* strains were re-infected by adding a colony of *Chlorella* from the plate stocks derived from the appropriate strain. This was done with all three of the isolated *Chlorella* strains to construct all possible host-symbiont genotype pairings (n=9). The regreening process was followed by microscopy and took between 2-6 weeks. Over the process, cells were grown at the intermediate light level of 12 µE m⁻² s⁻¹ and were given bacterized PPM weekly.

Diagnostic PCR

The correct algae genotype within the cross-infections was confirmed using diagnostic PCR. The *Chlorella* DNA was extracted by isolating the *Chlorella* and then using a standard 6% Chelex100 resin (Bio-Rad) extraction method. A nested PCR technique with overlapping, multiplex Chlorophyta specific primers were used as described by Hoshina et al.⁴¹. Standard PCR reactions were performed using Go Taq Green Master Mix (Promega) and 0.5 µmol L⁻¹ of the primer. The thermocycler programme was set to: 94°C for 5min, 30 cycles of (94°C for 30sec, 55°C for 30sec, 72°C for 60sec), and 5 min at 72°C.

Growth rate

Growth rates of the host-symbiont pairings were measured across a light gradient. The cells were washed and concentrated with a 11µm nylon mesh using sterile Volvic and re-suspended in bacterized PPM. The cultures were then split and acclimated to their treatment light condition (0, 12, 24, & 50 µE m⁻² s⁻¹) for five days. The cultures were then re-suspended in bacterized PPM to a target cell density of 150 cell mL⁻¹. Cell densities were measured at 0, 24, 48 and 72 hours by fixing 360µL of each cell culture, in triplicate, in 1% v/v glutaraldehyde in 96-well flat-bottomed micro-well plates. Images were taken with a plate reader (Tecan Spark 10M) and cell counts were made using an automated image analysis macro in ImageJ v1.50i⁴². The initial host-symbiont growth rate was measured over a period of three days.

Symbiont load

The symbiont load (i.e., the number of symbionts per host cell) was measured in cultures derived from the growth rate experiment so that the data could be integrated between the two measurements. Triplicate 300µl samples of each cell culture were taken from 72-hour cultures for flow cytometry analysis. Host symbiont load was estimated using a CytoFLEX S flow cytometer (Beckman Coulter Inc., CA, USA) by measuring the intensity of chlorophyll fluorescence for single *P. bursaria* cells (excitation 488nm, emission 690/50nm) and gating cell size using forward side scatter; a method established by Kadono et al.¹⁹. The measurements were calibrated against 8-peak rainbow calibration particles (BioLegend), and then presented as relative fluorescence to reduce variation across sampling sessions.

Partner switching

Metabolomics experiment

Cultures of the host-symbiont pairings were washed and concentrated with a 11µm nylon mesh using sterile Volvic and re-suspended in bacterized PPM. The cultures were then split and acclimated at their treatment light condition (0, 12 & 50 µE m⁻² s⁻¹) for seven days. The symbiotic partners were separated in order to get *P. bursaria* and *Chlorella* metabolic fraction. The *P. bursaria* cells were concentrated with a 11µm nylon mesh using Volvic and then the *P. bursaria* cells were disrupted by sonication (20% power for 10 secs). 1ml of the lysate was pushed through a 1.6µm filter, which caught the intact *Chlorella* cells, and the run-through was collected and stored as the *P. bursaria* fraction. The 1.6µm filter was washed with 5ml cold deionized water, and then reversed so that the *Chlorella* cells were resuspended in 1ml of cold methanol, which was stored as the *Chlorella* fraction. After which the *Chlorella* fraction samples were already in methanol, but the *P. bursaria* fraction samples had then to be diluted by 50% with methanol.

Mass spectrometry

Metabolic profiles were recorded using ESI ToF-MS, on the Qstar Elite with automatic injection using Waters Alliance 2695 HPLC (no column used), in positive mode. This is an established high-throughput method with a large mass range (50 Da to 1000 Da).

The mass spectrometry settings were: positive polarity, 4.2kV Ion Spray voltage, 120V Declustering potential, 265V Focusing potential, 200°C Source temperature, 40 ml min⁻¹ Gas Flow, the solvent was 50:50 methanol to water at flow rate 40 µl min⁻¹ and the injected volume was 10 µl.

The processing was performed using in-house software Visual Basic macro 216⁴³, which combined the spectra across the technical replicates by binning the crude m/z values into 0.2-unit bins. The relative mass abundances (% total ion count) for each bin was summed. Pareto scaling was applied to the results, and the data was then analysed by principal component analysis using SIMCA-P software (Umetrics). When treatment-based separation was observed, supervised orthogonal partial least squares discriminant analysis (OPLS-DA) separation was then performed using the discriminatory treatment with the SIMCA-P software.

Identification of significant masses

Masses of interest were annotated using the initial identifications from the in-house software program and further comparisons against KEGG (<https://www.genome.jp/kegg/>)^{44,45} and Metlin (<https://metlin.scripps.edu>)⁴⁶ databases. The Metabolomics Standards Initiative requires two independent measures to confirm identity, this partner-switching metabolomic analysis only used one measure (accurate mass) and therefore, meets only the level 2 requirements of putative annotated compounds.

Evolution Experiment

The populations used derive from the cross-infections and, therefore, the host-symbiont pairings come from the same cured 186b ancestor that was then re-infected with either its native (186b) or non-native (HK1) symbionts. The two host-symbiont pairings were split into six replicate populations that were used as the starting populations. The 200ml populations were propagated by weekly serial transfer for 25 transfers at a high light (50 µE m⁻² s⁻¹) 14:10 L:D cycle. At every transfer, cell-density was equalised to 100 cells mL⁻¹ and the transferred cells were washed with a 11 µm nylon mesh using Volvic before being re-suspended in bacterized PPM. Cell density was measured before and after each transfer by fixing 360 µL of each cell culture, in triplicate, in 1% v/v glutaraldehyde in 96-well flat-

bottomed micro-well plates. Images were taken with a plate reader (Tecan Spark 10M) and cell counts were made using an automated image analysis macro in ImageJ v1.50i⁴². Growth rate and symbiont load assays were conducted at the start, T10, T20 and end of the experiment using the method described above.

Fitness assay

Fitness assays were conducted at the start and end of the evolution experiment. *P. bursaria* cultures, both the symbiotic pairings and the symbiont-free ancestor, were washed with Volvic and resuspended in bacterized PPM. The cultures were then split and acclimated at their treatment light level (0,12,50 $\mu\text{E m}^{-2} \text{s}^{-1}$) for five days. Cell densities were counted by fixing 360 μL of each cell culture, in triplicate, in 1% v/v glutaraldehyde in 96-well flat-bottomed micro-well plates. Images were taken with a plate reader (Tecan Spark 10M) and cell counts were made using an automated image analysis macro in ImageJ v1.50i⁴². The competitions were started by setting up microcosms that each contained 50:50 populations of green and white cells (with target values of 20 green cells and 20 white cells per mL) that were in direct competition. Cells were sampled on day 0 and day 7 on a flow cytometer and the proportion of green to white cells was measured and used to calculate the selection rate. Selection rate (R) is calculated as the difference in Malthusian parameters of green (test) versus white (reference) cell populations in direct competition: $R = (\ln(\text{test}_{\text{start}}/\text{test}_{\text{end}}) - \ln(\text{reference}_{\text{start}}/\text{reference}_{\text{end}})) / \text{day}$ ⁴⁷. Green versus white cells were distinguished using single cell fluorescence estimated using a CytoFLEX S flow cytometer (Beckman Coulter Inc., CA, USA) by measuring the intensity of chlorophyll Fluorescence (excitation 488nm, emission 690/50nm) and gating cell size using forward side scatter; a method established by Kadono et al.¹⁹. The measurements were calibrated against 8-peak rainbow calibration particles (BioLegend), and then presented as relative fluorescence to reduce variation across sampling sessions. The re-establishment of endosymbiosis takes between 2-4 weeks, and this method was tested to ensure that the symbiont-free cells do not re-green over the course of the experiment.

Metabolomics

The cultures were sampled at the start and end of the evolution experiment. Cultures were washed and concentrated with a 11 μm nylon mesh using Volvic and re-suspended in bacterized PPM. The cultures were acclimated at their treatment light condition (50 $\mu\text{E m}^{-2} \text{s}^{-1}$) for seven days. At the start of the evolution experiment we analysed a sample from each of the 6 replicate populations per treatment to determine the ancestral metabolomes of each host-symbiont pairing (i.e., n=6). At the end of the evolution experiment, we increased our replication such that for each of the 6 replicate populations per treatment we analysed 3

technical replicates, allowing us to determine differences between replicate populations as well as between treatments in their evolved metabolomes. At each sampling event, the symbiotic partners were separated in order to get *P. bursaria* and *Chlorella* metabolic fraction using the extraction method described above. Samples were freeze-dried for storage, and then resuspended in 50:50 methanol to water prior to mass spectrometry.

The samples were analysed with a Synapt G2-Si with Acuity UPLC, recording in positive mode over a large untargeted mass range (50 – 1000 Da). A 2.1x50mm Acuity UPLC BEH C18 column was used with acetonitrile as the solvent. The machine settings are listed in detail below:

The mass spectrometry settings were: positive polarity, 2.3kV Capillary voltage, 20V Sample Cone voltage, 100°C Source Temperature, 280°C Desolvation temperature, 600 L hr⁻¹ Gas Flow, 5µl Injected volume and 45°C Column temperature. The gradient started at time 0 with 95% water to 5% acetonitrile, at 3 minutes it was 65% water to 35% acetonitrile, at 6 minutes it was 0% water to 100% acetonitrile, at 7.5 minutes it was 0% water to 100% acetonitrile, and at 7.6 minutes it was 95% water to 5% acetonitrile.

The *P. bursaria* and *Chlorella* fraction were analysed separately. The xcms R package^{48–50} was used to extract the spectra from the CDF data files, using a step argument of 0.01 m/z. Peaks were identified, and then grouped across samples. These aligned peaks were used to identify and correct correlated drifts in retention time from run to run. Pareto scaling was applied to the resulting intensity matrix.

Metabolomics analysis

The metabolic profiles from the start and end of the experiment were compared using principal component analysis (PCA) with the prcomp() function in Base R (<https://www.rproject.org/>). For both fractions the first three components were considered, this accounted for >88% of the variance. The top 1% of the loadings were selected using the absolute magnitude of the loadings. These top loadings were identified where possible, and the identified loadings were then depicted in their associated component space. The relative abundance of these top loadings was visualised using heatmaps drawn with the heatmap.2() function from the gplot package⁵¹. The phylogenies were based on UPGMA clustering of the PCA coordinates of the samples using the hclust() function. This approach of integrating metabolic data and genotypes in heatmaps has been used previously⁵².

Identification of significant masses

Masses of interest were investigated using the MarVis-Suite 2.0 software (<http://marvis.gobics.de/>)⁵³, using retention time and mass to compare against KEGG (<https://www.genome.jp/kegg/>)^{44,45} and MetaCyc (<https://biocyc.org/>)⁵⁴ databases. The Metabolomics Standards Initiative requires two independent measures to confirm identity, which the combination of retention time and accurate mass achieves for the analysis of the evolution experiment metabolomics.

Quantification and Statistical analysis

Statistical analyses were performed in Rv.3.5.0⁵⁵ and all plots were produced using package ggplot2⁵⁶ unless otherwise stated. Physiology tests were analysed by both ANOVA and ANCOVA, with transfer time, host and symbiont identity as factors. A linear mixed effect model was used to analysis the growth rate per transfer using lm() function from the nlme package⁵⁷. The lm model included fixed effects of symbiont genotype and transfer number, and random effects of transfer number given sample ID. Where parametric tests were used the data conformed to parametric assumptions of independence, normality and homogeneity of variance, which was confirmed using the appropriate tests and plots (e.g normal QQ and residual vs fitted values). Summary details of the data is provided in the figure legends (e.g the value of n and type of error used) and details of the statistical methods used are within the supplementary statistics data (Data S1).

Within all of our experiments the spatial arrangement of cultures in the incubator was fully randomised to ensure statistical independence. For the short term assays the spatial randomisation was reassigned every day. For the long-term evolution experiment the spatial randomisation was reassigned at each weekly serial transfer.

Supplementary data file legend

Data S1. Statistical outputs and model parameters for analyses associated with the figures of the main manuscript and supplementary figures. Related to Figures 1-3 & S3 and STAR Methods.

A.) Data S1A is related to Figure 1: the first section presents an ANOVA and Welch two sample t-test related to Figure 1A, the second section presents an ANOVA and polynomial model related to Figure 1B. B.) Data S1B presents an ANOVA model related to Figure 2. C) Data S1C presents an ANOVA model related to Figure 3. D) Data S1D is related to Figure S3: the first section presents a linear mixed effect model related to Figure S3A, the second

section presents a Welch two sample t-test related to Figure S3B. In all relevant statistical models, light is treated as a continuous variable.

References:

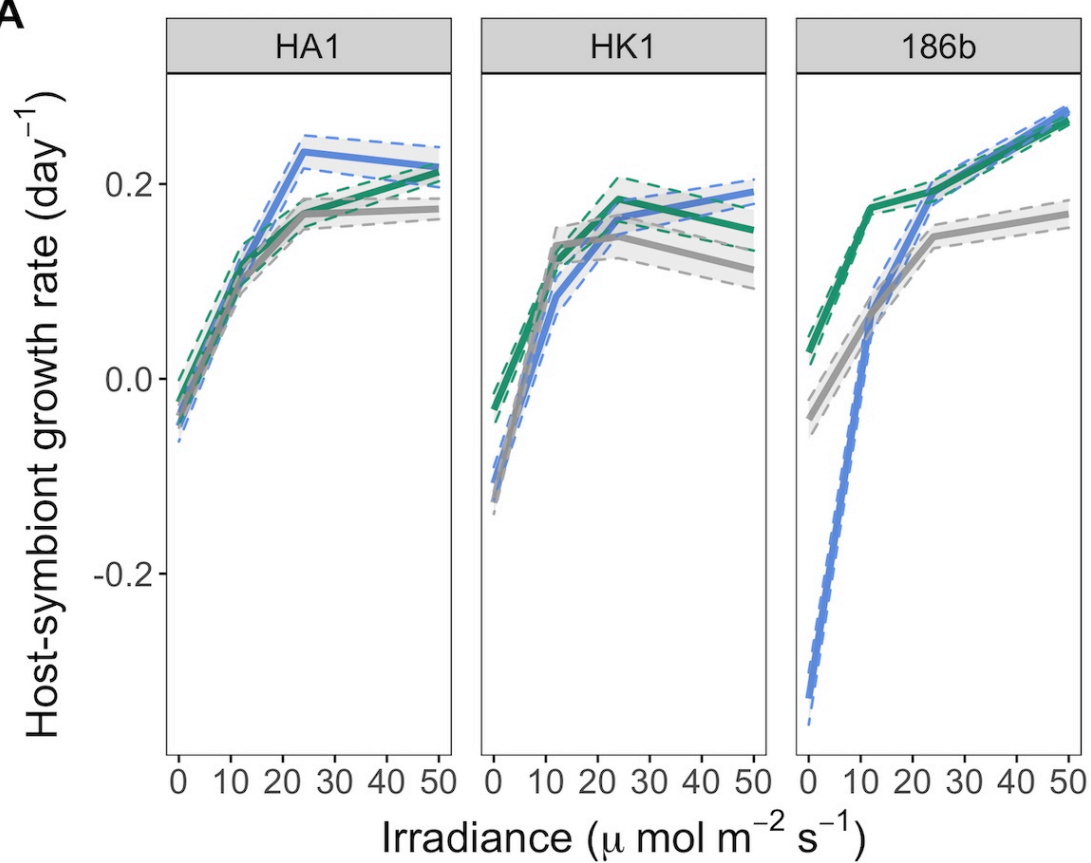
1. Sachs, J.L., and Simms, E.L. (2006). Pathways to mutualism breakdown. *Trends in Ecology & Evolution* 21, 585–592.
2. Boulotte, N.M., Dalton, S.J., Carroll, A.G., Harrison, P.L., Putnam, H.M., Peplow, L.M., and van Oppen, M.J. (2016). Exploring the *Symbiodinium* rare biosphere provides evidence for symbiont switching in reef-building corals. *The ISME Journal* 10, 2693–2701.
3. Lefèvre, C., Charles, H., Vallier, A., Delobel, B., Farrell, B., and Heddi, A. (2004). Endosymbiont Phylogenesis in the Dryophthoridae Weevils: Evidence for Bacterial Replacement. *Mol Biol Evol* 21, 965–973.
4. Koga, R., and Moran, N.A. (2014). Swapping symbionts in spittlebugs: evolutionary replacement of a reduced genome symbiont. *The ISME Journal* 8, 1237–1246.
5. Matsuura, Y., Moriyama, M., Łukasik, P., Vanderpool, D., Tanahashi, M., Meng, X.-Y., McCutcheon, J.P., and Fukatsu, T. (2018). Recurrent symbiont recruitment from fungal parasites in cicadas. *PNAS* 115, E5970–E5979.
6. Heath, K.D. (2010). Intergenomic Epistasis and Coevolutionary Constraint in Plants and Rhizobia. *Evolution* 64, 1446–1458.
7. Thompson, J.N. (2005). *The Geographic Mosaic of Coevolution* (University of Chicago Press).
8. Heath, K.D., and Tiffin, P. (2007). Context dependence in the coevolution of plant and rhizobial mutualists. *Proceedings of the Royal Society of London B: Biological Sciences* 274, 1905–1912.
9. Joy, J.B. (2013). Symbiosis catalyses niche expansion and diversification. *Proceedings of the Royal Society B: Biological Sciences* 280, 20122820.
10. Sudakaran, S., Kost, C., and Kaltenpoth, M. (2017). Symbiont Acquisition and Replacement as a Source of Ecological Innovation. *Trends in Microbiology* 25, 375–390.
11. Jaenike, J., Unckless, R., Cockburn, S.N., Boelio, L.M., and Perlman, S.J. (2010). Adaptation via Symbiosis: Recent Spread of a *Drosophila* Defensive Symbiont. *Science* 329, 212–215.
12. Jiggins, F.M., and Hurst, G.D.D. (2011). Rapid Insect Evolution by Symbiont Transfer. *Science* 332, 185–186.

- 635 13. Matthews, J.L., Oakley, C.A., Lutz, A., Hillyer, K.E., Roessner, U., Grossman, A.R.,
636 Weis, V.M., and Davy, S.K. (2018). Partner switching and metabolic flux in a model
637 cnidarian–dinoflagellate symbiosis. *Proceedings of the Royal Society B: Biological*
638 *Sciences* 285, 20182336.
- 639 14. Russell, J.A., and Moran, N.A. (2005). Horizontal Transfer of Bacterial Symbionts:
640 Heritability and Fitness Effects in a Novel Aphid Host. *Appl. Environ. Microbiol.* 71,
641 7987–7994.
- 642 15. McGraw, E.A., Merritt, D.J., Droller, J.N., and O'Neill, S.L. (2002). Wolbachia density
643 and virulence attenuation after transfer into a novel host. *PNAS* 99, 2918–2923.
- 644 16. Nakayama, S., Parratt, S.R., Hutchence, K.J., Lewis, Z., Price, T. a. R., and Hurst,
645 G.D.D. (2015). Can maternally inherited endosymbionts adapt to a novel host? Direct
646 costs of *Spiroplasma* infection, but not vertical transmission efficiency, evolve rapidly
647 after horizontal transfer into *D. melanogaster*. *Heredity* 114, 539–543.
- 648 17. Sullivan, J.T., Patrick, H.N., Lowther, W.L., Scott, D.B., and Ronson, C.W. (1995).
649 Nodulating strains of *Rhizobium loti* arise through chromosomal symbiotic gene transfer
650 in the environment. *PNAS* 92, 8985–8989.
- 651 18. Johnson, M.D. (2011). The acquisition of phototrophy: adaptive strategies of hosting
652 endosymbionts and organelles. *Photosynth Res* 107, 117–132.
- 653 19. Kadono, T., Kawano, T., Hosoya, H., and Kosaka, T. (2004). Flow cytometric studies of
654 the host-regulated cell cycle in algae symbiotic with green paramecium. *Protoplasma*
655 223, 133–141.
- 656 20. Ziesenisz, E., Reisser, W., and Wiessner, W. (1981). Evidence of de novo synthesis of
657 maltose excreted by the endosymbiotic *Chlorella* from *Paramecium bursaria*. *Planta* 153,
658 481–485.
- 659 21. Kodama, Y., and Fujishima, M. (2011). Four important cytological events needed to
660 establish endosymbiosis of symbiotic *Chlorella* sp. to the alga-free *Paramecium*
661 *bursaria*. *Japanese Journal of Protozoology* 44, 1–20.
- 662 22. Siegel, R.W. (1960). Hereditary endosymbiosis in *Paramecium bursaria*. *Experimental*
663 *Cell Research* 19, 239–252.
- 664 23. Sørensen, M.E., Wood, A.J., Minter, E.J., Lowe, C.D., Cameron, D.D., and Brockhurst,
665 M.A. (2020). Comparison of independent evolutionary origins reveals both convergence
666 and divergence in the metabolic mechanisms of symbiosis. *Current Biology*.
- 667 24. Lowe, C.D., Minter, E.J., Cameron, D.D., and Brockhurst, M.A. (2016). Shining a Light
668 on Exploitative Host Control in a Photosynthetic Endosymbiosis. *Current Biology* 26,
669 207–211.
- 670 25. Dean, A.D., Minter, E.J.A., Sørensen, M.E.S., Lowe, C.D., Cameron, D.D., Brockhurst,
671 M.A., and Jamie Wood, A. (2016). Host control and nutrient trading in a photosynthetic
672 symbiosis. *Journal of Theoretical Biology* 405, 82–93.
- 673 26. Minter, E.J.A., Lowe, C.D., Sørensen, M.E.S., Wood, A.J., Cameron, D.D., and
674 Brockhurst, M.A. (2018). Variation and asymmetry in host-symbiont dependence in a
675 microbial symbiosis. *BMC Evol Biol* 18, 108.

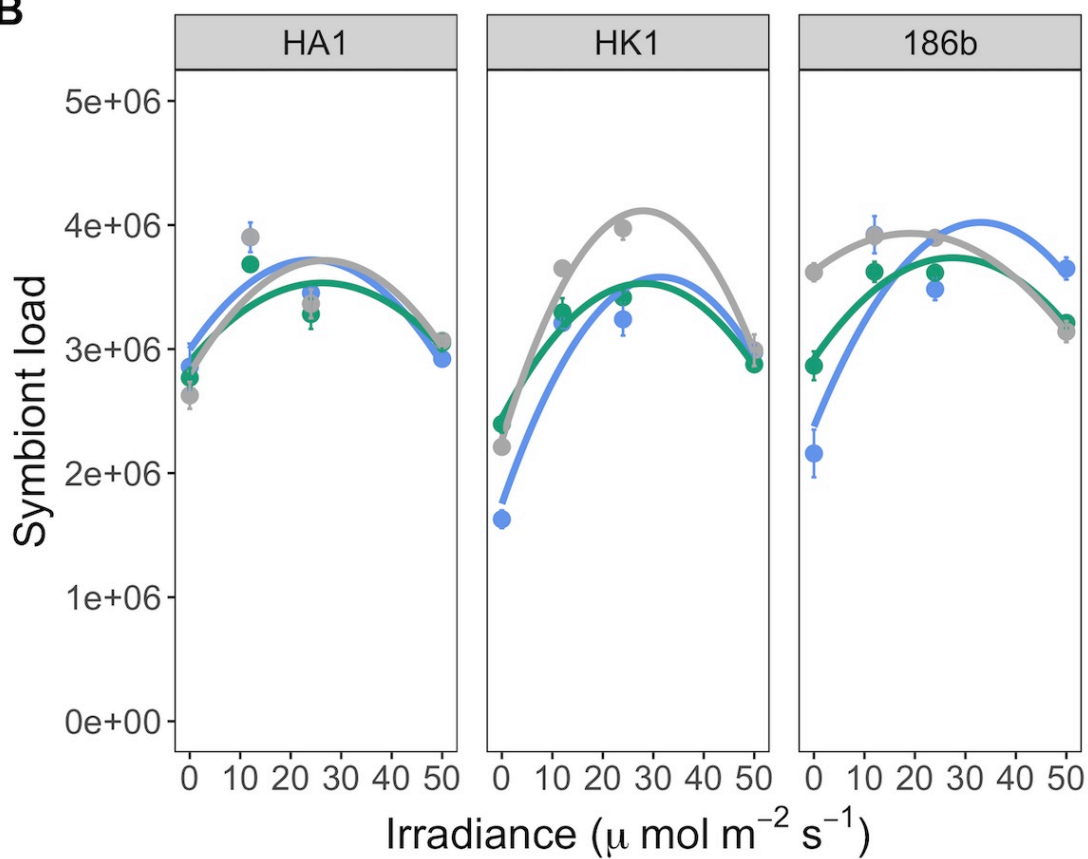
- 676 27. Mallick, N. (2004). Copper-induced oxidative stress in the chlorophycean microalga
677 *Chlorella vulgaris*: response of the antioxidant system. *J. Plant Physiol.* *161*, 591–597.
- 678 28. Shiu, C.-T., and Lee, T.-M. (2005). Ultraviolet-B-induced oxidative stress and responses
679 of the ascorbate-glutathione cycle in a marine macroalga *Ulva fasciata*. *J. Exp. Bot.* *56*,
680 2851–2865.
- 681 29. Kodama, Y., and Fujishima, M. (2008). Cycloheximide Induces Synchronous Swelling of
682 Perialgal Vacuoles Enclosing Symbiotic *Chlorella vulgaris* and Digestion of the Algae in
683 the Ciliate *Paramecium bursaria*. *Protist* *159*, 483–494.
- 684 30. Kodama, Y., and Fujishima, M. (2012). Cell division and density of symbiotic *Chlorella*
685 *variabilis* of the ciliate *Paramecium bursaria* is controlled by the host's nutritional
686 conditions during early infection process. *Environmental Microbiology* *14*, 2800–2811.
- 687 31. Cantin, N.E., van Oppen, M.J.H., Willis, B.L., Mieog, J.C., and Negri, A.P. (2009).
688 Juvenile corals can acquire more carbon from high-performance algal symbionts. *Coral*
689 *Reefs* *28*, 405.
- 690 32. Freeman, C.J., Thacker, R.W., Baker, D.M., and Fogel, M.L. (2013). Quality or quantity:
691 is nutrient transfer driven more by symbiont identity and productivity than by symbiont
692 abundance? *The ISME Journal* *7*, 1116–1125.
- 693 33. Husnik, F., and McCutcheon, J.P. (2016). Repeated replacement of an intrabacterial
694 symbiont in the tripartite nested mealybug symbiosis. *PNAS* *113*, E5416–E5424.
- 695 34. Rolshausen, G., Grande, F.D., Sadowska-Deś, A.D., Otte, J., and Schmitt, I. (2018).
696 Quantifying the climatic niche of symbiont partners in a lichen symbiosis indicates
697 mutualist-mediated niche expansions. *Ecography* *41*, 1380–1392.
- 698 35. Matthews, J.L., Oakley, C.A., Lutz, A., Hillyer, K.E., Roessner, U., Grossman, A.R.,
699 Weis, V.M., and Davy, S.K. (2018). Partner switching and metabolic flux in a model
700 cnidarian–dinoflagellate symbiosis. *Proceedings of the Royal Society B: Biological*
701 *Sciences* *285*, 20182336.
- 702 36. Weis, V.M. (2008). Cellular mechanisms of Cnidarian bleaching: stress causes the
703 collapse of symbiosis. *Journal of Experimental Biology* *211*, 3059–3066.
- 704 37. Abrego, D., Ulstrup, K.E., Willis, B.L., and van Oppen, M.J.H. (2008). Species–specific
705 interactions between algal endosymbionts and coral hosts define their bleaching
706 response to heat and light stress. *Proceedings of the Royal Society B: Biological*
707 *Sciences* *275*, 2273–2282.
- 708 38. Ye, S., Bhattacharjee, M., and Siemann, E. (2019). Thermal Tolerance in Green Hydra:
709 Identifying the Roles of Algal Endosymbionts and Hosts in a Freshwater Holobiont Under
710 Stress. *Microb Ecol* *77*, 537–545.
- 711 39. Howells, E.J., Beltran, V.H., Larsen, N.W., Bay, L.K., Willis, B.L., and van Oppen, M.J.H.
712 (2012). Coral thermal tolerance shaped by local adaptation of photosymbionts. *Nature*
713 *Climate Change* *2*, 116–120.
- 714 40. Stein, J.R. (1979). (ED.) *Handbook of Phycological Methods: Culture Methods and*
715 *Growth Measurements* (Cambridge University Press).

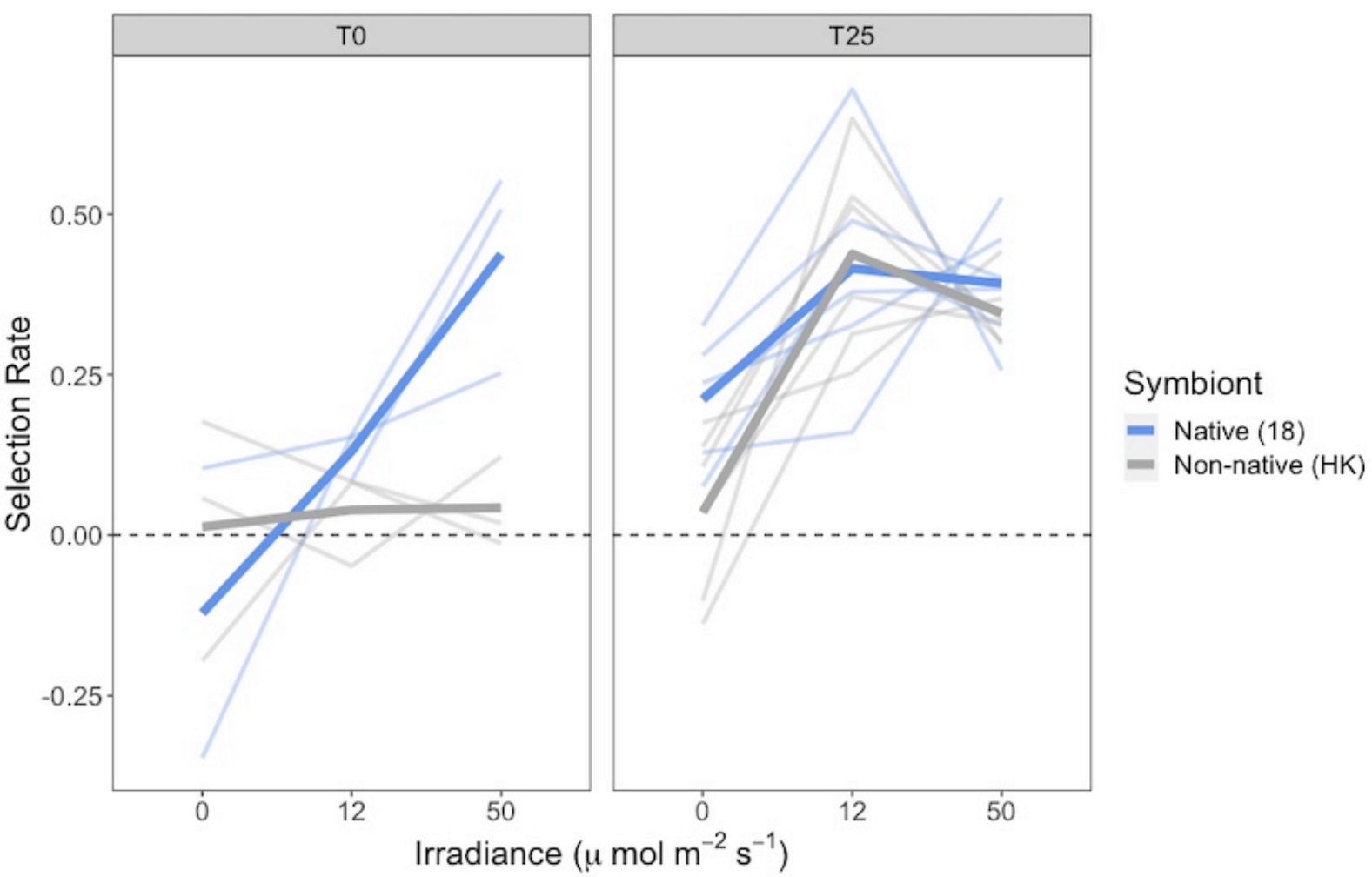
- 716 41. Hoshina, R., Kato, Y., Kamako, S., and Imamura, N. (2005). Genetic Evidence of
717 “American” and “European” Type Symbiotic Algae of *Paramecium bursaria* Ehrenberg.
718 *Plant Biol (Stuttg)* 7, 526–532.
- 719 42. Schneider, C.A., Rasband, W.S., and Eliceiri, K.W. (2012). NIH Image to ImageJ: 25
720 years of image analysis. *Nature Methods*. <https://www.nature.com/articles/nmeth.2089>.
- 721 43. Overy, S.A., Walker, H.J., Malone, S., Howard, T.P., Baxter, C.J., Sweetlove, L.J., Hill,
722 S.A., and Quick, W.P. (2005). Application of metabolite profiling to the identification of
723 traits in a population of tomato introgression lines. *J Exp Bot* 56, 287–296.
- 724 44. Kanehisa, M., and Goto, S. (2000). KEGG: kyoto encyclopedia of genes and genomes.
725 *Nucleic Acids Res.* 28, 27–30.
- 726 45. Kanehisa, M., Sato, Y., Furumichi, M., Morishima, K., and Tanabe, M. (2019). New
727 approach for understanding genome variations in KEGG. *Nucleic Acids Res.* 47, D590–
728 D595.
- 729 46. Smith, C.A., O’Maille, G., Want, E.J., Qin, C., Trauger, S.A., Brandon, T.R., Custodio,
730 D.E., Abagyan, R., and Siuzdak, G. (2005). METLIN: a metabolite mass spectral
731 database. *Ther Drug Monit* 27, 747–751.
- 732 47. Lenski, R.E., Rose, M.R., Simpson, S.C., and Tadler, S.C. (1991). Long-Term
733 Experimental Evolution in *Escherichia coli*. I. Adaptation and Divergence During 2,000
734 Generations. *The American Naturalist* 138, 1315–1341.
- 735 48. Benton, H.P., Want, E.J., and Ebbels, T.M.D. (2010). Correction of mass calibration
736 gaps in liquid chromatography-mass spectrometry metabolomics data. *Bioinformatics*
737 26, 2488–2489.
- 738 49. Smith, C.A., Want, E.J., O’Maille, G., Abagyan, R., and Siuzdak, G. (2006). XCMS:
739 Processing Mass Spectrometry Data for Metabolite Profiling Using Nonlinear Peak
740 Alignment, Matching, and Identification. *Anal. Chem.* 78, 779–787.
- 741 50. Tautenhahn, R., Böttcher, C., and Neumann, S. (2008). Highly sensitive feature
742 detection for high resolution LC/MS. *BMC Bioinformatics* 9, 504.
- 743 51. Warnes, G.R., Bolker, B., Bonebakker, L., Gentleman, R., Huber, W., Liaw, A., Lumley,
744 T., Maechler, M., Magnusson, A., and Moeller, S. (2009). gplots: Various R programming
745 tools for plotting data. R package version 2, 1.
- 746 52. Cotton, T.E.A., Pétriacq, P., Cameron, D.D., Meselmani, M.A., Schwarzenbacher, R.,
747 Rolfe, S.A., and Ton, J. (2019). Metabolic regulation of the maize rhizobiome by
748 benzoxazinoids. *ISME J* 13, 1647–1658.
- 749 53. Kaefer, A., Lingner, T., Feussner, K., Göbel, C., Feussner, I., and Meinicke, P. (2009).
750 MarVis: a tool for clustering and visualization of metabolic biomarkers. *BMC*
751 *Bioinformatics* 10, 92.
- 752 54. Caspi, R., Billington, R., Fulcher, C.A., Keseler, I.M., Kothari, A., Krummenacker, M.,
753 Latendresse, M., Midford, P.E., Ong, Q., Ong, W.K., et al. (2018). The MetaCyc
754 database of metabolic pathways and enzymes. *Nucleic Acids Res* 46, D633–D639.
- 755 55. R Core Team (2018). R: A Language and Environment for Statistical Computing.

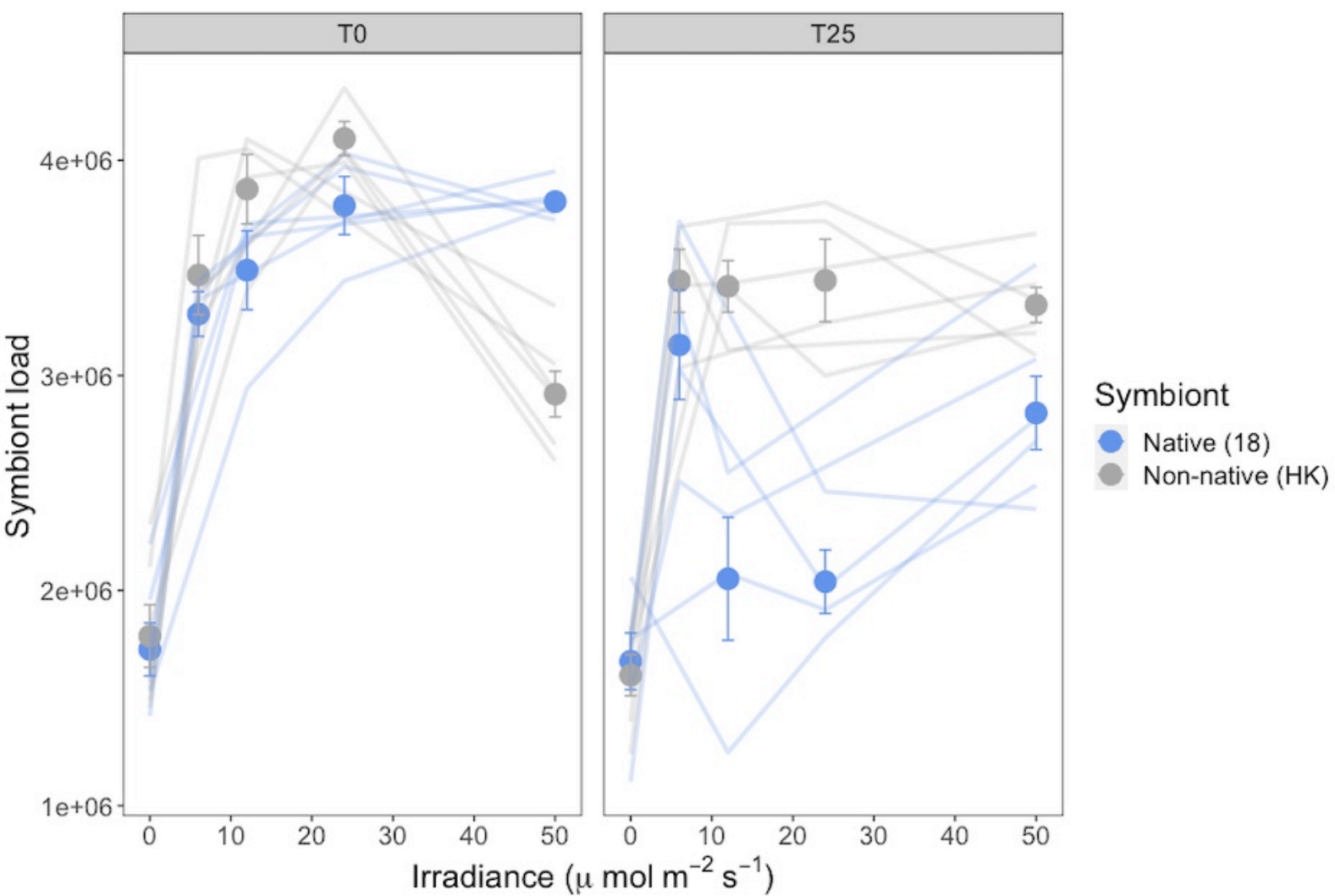
- 756 56. Wickham, H. (2016). ggplot2: Elegant Graphics for Data Analysis.
- 757 57. Pinheiro, J., Bates, D., DebRoy, S., Sarkar, D., and R core Team (2019) (2019). nlme:
758 Linear and Nonlinear Mixed Effects Models.
- 759

A

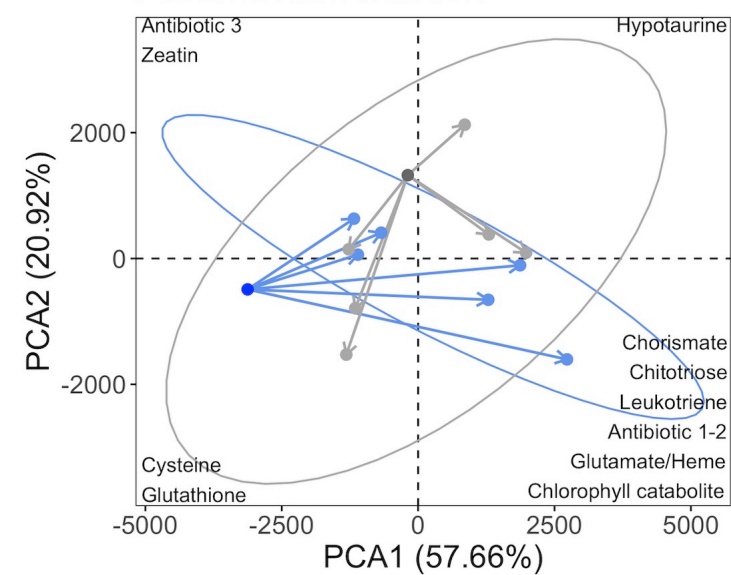
Symbiont genotype

**B**

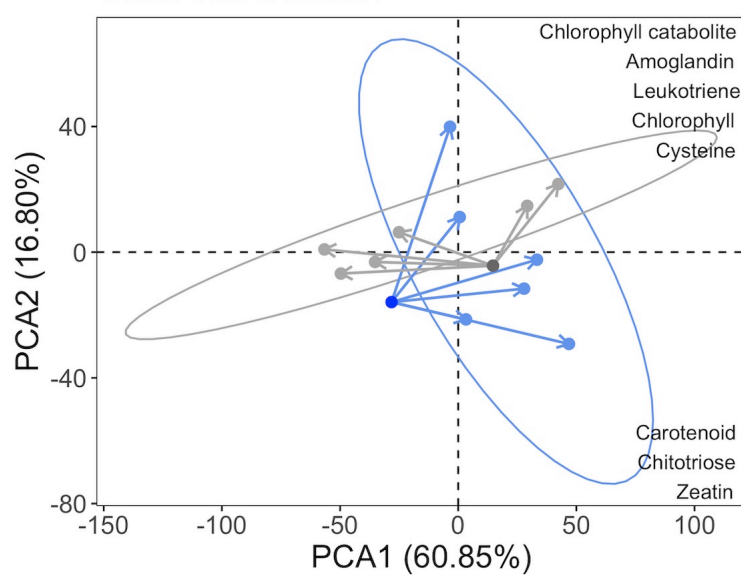




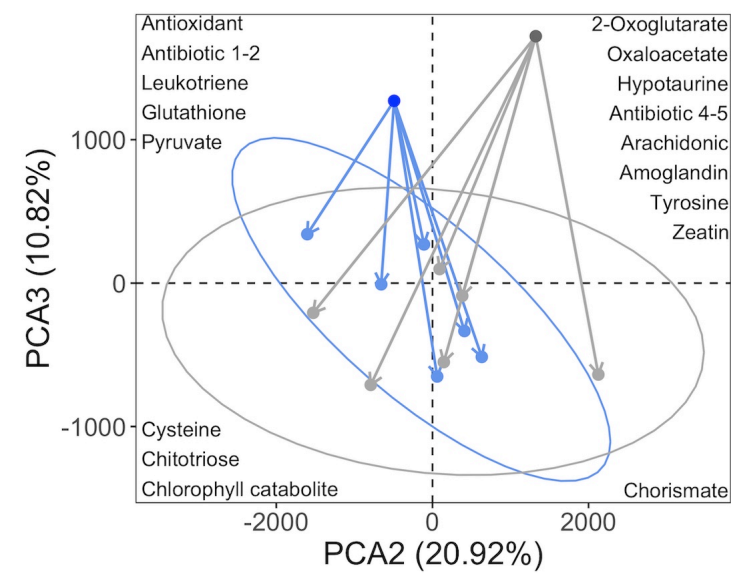
A Paramecium fraction



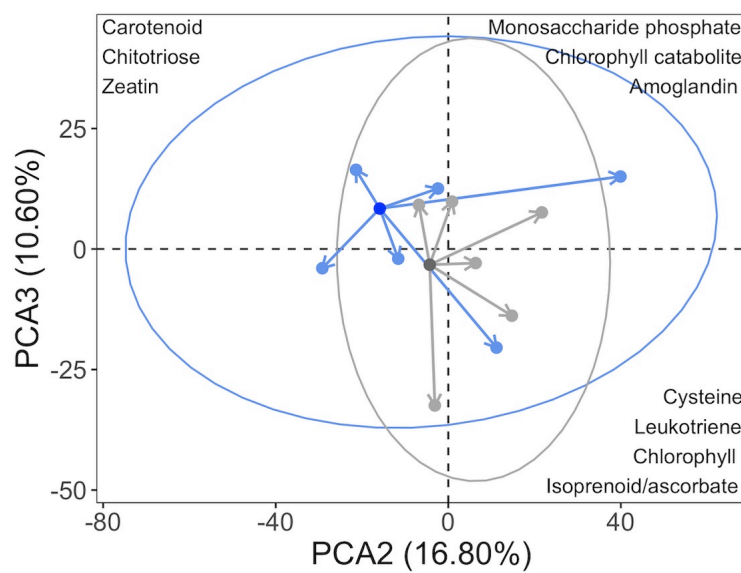
B Chlorella fraction



C Paramecium fraction



D Chlorella fraction



Group 18 18start HK HKstart